

# Designed self-assembly of programmable colloidal atom-electron equivalents

Xiuyang Xia,<sup>1,2,\*</sup> Yuhan Peng,<sup>1,\*</sup> Ka Ki Li,<sup>3</sup> and Ran Ni<sup>1,†</sup>

<sup>1</sup> School of Chemistry, Chemical Engineering and Biotechnology,  
Nanyang Technological University, 62 Nanyang Drive, 637459, Singapore

<sup>2</sup> Arnold Sommerfeld Center for Theoretical Physics and Center for NanoScience,  
Department of Physics, Ludwig-Maximilians-Universität München,  
Theresienstraße 37, D-80333 München, Germany

<sup>3</sup> Department of Mathematics, Hong Kong University of Science and Technology,  
Clear Water Bay, Hong Kong

To unlock the potential for assembling complex colloidal “molecules”, we investigate a minimal binary system of programmable colloidal atom–electron equivalents (PAE-EE), where electron equivalents (EEs) are multivalent linkers with two distinct types of single-stranded DNA (ssDNA) ends complementary to those ssDNAs on binary programmable atom equivalents (PAEs). We derive a statistical mechanical framework for calculating the effective interaction between PAEs mediated by EEs with arbitrary valency, which quantitatively agrees with simulations that explicitly include EEs. Our analysis reveals an anomalous dependence of PAE-PAE interactions on the EE valency, showing that EE-mediated interactions converge at the large valency limit. Moreover, we identify an optimal EE valency that maximizes the interaction difference between targeted and non-targeted binding pairs of PAEs. These findings offer design principles for targeted self-assembly in PAE-EE systems.

DNA-based materials enable the self-assembly of complex and programmable structures through the precise molecular recognition capabilities of DNA [1]. By attaching single-stranded DNAs (ssDNAs) to colloidal surfaces, DNA-coated particles facilitate the formation of organized superstructures [2–4], where the dual designability of DNA-encoded targeted structures and colloidal properties allows for the emulation of complex biological processes, merging biological sciences with material engineering, e.g., leading to applications in drug delivery [5, 6], biosensing [7–9] and immunotherapy [10, 11].

The linker-mediated scheme introduces additional designability for orthogonally regulating the specificity of pair interactions [12–17]. Moreover, multivalent linkers, or termed electron equivalents (EEs), in these systems exhibit behavior analogous to electrons in metals, roaming through colloidal crystals and fostering effective attraction between larger DNA-coated colloids, termed programmable atom equivalents (PAEs) [18]. This system serves as a colloidal analog to atoms and electrons, manifesting phenomena such as EE localization similar to the metal-insulator transition [18–22], the emergence of coordination numbers [23, 24], and the formation of colloidal alloys [25] and colloidal superionic conductors [26].

Existing programmable atom-electron equivalent (PAE-EE) systems have primarily utilized EEs that are multivalent linkers with identical ssDNA ends. However, this homogeneity limits the complexity of the resulting assemblies. For more sophisticated structures, such as colloidal “molecules”, it is essential to employ EEs with heterogeneous ends to guide programmable assembly. In this Letter, we investigate a minimal binary PAE-EE system, where the EEs possess two distinct types of ends complementary with the ssDNA ends on binary PAEs. We derive an explicit formula for calculating the effective

interaction between PAEs mediated by EEs of *arbitrary* valency from a statistical mechanical model based on the quantitative model for DNA-coated colloids [16, 27–29]. This approach captures the interplay among binding energy, configurational entropy, and combinatorial entropy, allowing us to study the distribution of EEs in different binding states, which serves as a framework for Monte Carlo (MC) simulations with implicit EEs. We study the EE-mediated pair interaction between the same and different types of PAEs and corresponding phase behaviors, offering a design principle to guide the targeted self-assembly in PAE-EE systems.

*Model and EE-mediated interactions.* We consider an  $\alpha\gamma$ -type binary PAE system in a solution containing free EEs, and each PAE is modeled as a hard sphere of radius  $R$  coated with  $n_\alpha$   $\alpha$ -type or  $n_\gamma$   $\gamma$ -type mobile ssDNA ends (Fig. 1(a)). The mobility of ssDNAs coated on PAEs allows treating them as a mean-field-like adsorption layer to derive a closed form for effective interactions, and does not change the qualitative physics in the system [28]. ssDNA ends are modeled as infinitely thin, hard rods of length  $l_r$ . Free EEs bridge PAEs in the solution and are connected to a reservoir of chemical potential  $\mu$ . Each EE is modeled as a polymer blob of zero radius, which is based on the fact that EEs are normally much smaller than PAEs experimentally. An EE consists of equimolar  $\lambda$  number of  $\alpha'$  and  $\gamma'$ -type ends, which are complementary to the  $\alpha$  and  $\gamma$ -type ssDNAs coated on colloids, respectively. We set the binding energy as  $\Delta G_{\alpha\alpha'} = \Delta G_{\gamma\gamma'} = \Delta G$ , which characterizes the chemical details of specific binding. Non-specific bindings between  $\alpha-\gamma$ ,  $\alpha-\gamma'$ ,  $\alpha'-\gamma$ , and  $\alpha'-\gamma'$  ends are neglected.

In typical experimental PAE-EE systems, van der Waals interactions and electrostatic interactions can be

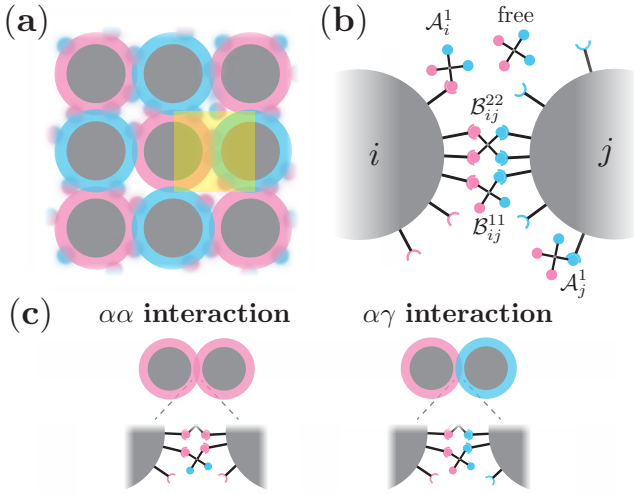


FIG. 1: **Programmable colloidal atom-electron equivalents.** (a) Schematic representation of binary PAEs, where the PAE-PAE interaction is mediated via the bridging of free EEs binding with ssDNAs on PAEs. (b) A magnification of the yellow region in (a). Mobile ssDNA ends (red or blue hooks) coated on PAEs can bind with the ends (red or blue spheres) of free EEs of the same color. EEs can stay in different binding substates characterized by the number of bound ends. (c) Schematic representation of two types of interactions in the system: non-targeted  $\alpha\alpha$  interaction between the same type of PAEs and targeted  $\alpha\gamma$  interaction between the different types of PAEs.

neglected [30]. Besides, we also neglect the depletion interaction originating from the EEs acting as depletants, particularly when EEs are sufficiently small. Based on the fact that PAEs are much larger than EEs [18], we assume that the motion of PAEs and EEs can be decoupled, and EEs move within the static external potential generated by PAEs and provide effective interactions among PAEs. Consequently, PAEs interact mainly through entropic repulsion and EE-mediated attraction:

$$\beta U_{\text{eff}} = \beta F_{\text{att}} - \beta F'_{\text{att}} + \beta F_{\text{rep}}, \quad (1)$$

where  $F_{\text{att}}$  is the free energy of EEs given the coordinations of PAEs, and  $F'_{\text{att}}$  represents the free energy of EEs for isolated PAE configurations. The entropic repulsion  $\beta F_{\text{rep}}$  originates from the excluded volume of ssDNAs overlapping with the hard cores of PAEs [28]. Here  $\beta = 1/k_B T$  with  $k_B$  and  $T$  the Boltzmann constant and the temperature of the system, respectively. As shown in Fig. 1(c), we consider  $\beta U_{\text{eff}}^{\alpha\gamma/\alpha\alpha}$  to be the targeted/non-targeted PAE-PAE interaction, respectively.

As EEs are much smaller than PAEs, we assume that each EE can only be adsorbed onto one PAE  $i$  (adsorbed state  $\mathcal{A}_i$ ) or bridge between PAE  $i$  and  $j$  (bridging state  $\mathcal{B}_{ij}$ ). We note that the EEs here can exhibit different binding substates characterized by the number of bound ends. As shown in Fig. 1(b), we denote  $\mathcal{A}_i^k$  substate as  $k$  ends on an EE binding with the ends on particle  $i$ ,

and  $\mathcal{B}_{ij}^{kl}$  substate as  $k$  and  $l$  ends on an EE binding with the ends on PAE  $i$  and  $j$ , respectively. Using the saddle-point approximation, we obtain the equilibrium number of EEs,  $m_i^k$  and  $q_{ij}^{kl}$ , in different substates,  $\mathcal{A}_i^k$  and  $\mathcal{B}_{ij}^{kl}$ , respectively (see SM Sec. I [31])

$$m_i^k = (\bar{n}_i)^k \Xi_{\mathcal{A},i}^k, \quad q_{ij}^{kl} = (\bar{n}_i)^k (\bar{n}_j)^l \Xi_{\mathcal{B},ij}^{kl}, \quad (2)$$

where  $\bar{n}_i$  is the number of unbound ends on PAE  $i$ :

$$\bar{n}_i = n_i - \sum_k k m_i^k - \sum_j \sum_{k,l} k q_{ij}^{kl}. \quad (3)$$

The binding strength of an EE in  $\mathcal{A}_i^k$  substate,  $\Xi_{\mathcal{A},i}^k$ , and in  $\mathcal{B}_{ij}^{kl}$  substate,  $\Xi_{\mathcal{B},ij}^{kl}$ , can be written as

$$\Xi_{\mathcal{A},i}^k = m_i^0 \binom{\lambda}{k} (\chi_i)^k, \quad (4a)$$

$$\Xi_{\mathcal{B},ij}^{kl} = m_{ij}^0 w^{kl} (\chi_i)^k (\chi_j)^l, \quad (4b)$$

where  $m_i^0$  is the number of unbound EEs in the adsorption layer of PAE  $i$ , while  $m_{ij}^0$  is the number of unbound EEs in the overlapped adsorption layers between PAE  $i$  and  $j$ .  $\chi_i$  denotes the individual binding strength of each pair of ends binding between PAE  $i$  and an EE, which counts both energy and entropy effects. The combinatorial term in bridging  $w^{kl} = \binom{\lambda}{k,l}$  if  $t_i = t_j$ , while  $w^{kl} = \binom{\lambda}{k} \binom{\lambda}{l}$  if  $t_i \neq t_j$ , with  $t_{i/j}$  the type of PAE  $i/j$ . The free energy of bound EEs is given by

$$\beta F_{\text{att}} = \sum_i \left( n_i \log \bar{n}_i - \bar{n}_i - M_i - \sum_{j < i} Q_{ij} \right) + \text{const}, \quad (5)$$

where  $M_i$  and  $Q_{ij}$  are total numbers of EEs in the adsorbed state  $\mathcal{A}_i$  and bridging state  $\mathcal{B}_{ij}$ , respectively, and the constant indicates the reference to different configurations of PAEs. We notice that Eq. 3 can be numerically solved, and  $M_i$  and  $Q_{ij}$  in Eq. 5 are in closed forms for arbitrary  $\lambda$  (see SM Sec. I [31]).

*Numerical verification.* We aim to guide the targeted binding between  $\alpha$  and  $\gamma$  type PAEs through EE-mediated interactions. However, as shown in Fig. 1(c), due to the multivalency of EEs, non-targeted interactions exist between particles of the same type. Our goal is to understand how to design these interactions to optimize the ability to form targeted structures. We first perform grand canonical Monte Carlo (GCMC) simulations incorporating explicit EEs to validate the pair interactions. In our simulations, PAEs are modeled as mobile DNA-coated colloids (mDNACCs), while the EEs are treated as zero-volume mDNACCs that can interact with both  $\alpha$  and  $\gamma$  types. The interactions within the system are calculated based on the framework of reversible mobile binders proposed in Ref. [28]. Two PAEs of the same ( $\alpha\alpha$ ) or different types ( $\alpha\gamma$ ) are placed at fixed positions within a simulation box, while the EEs are inserted and

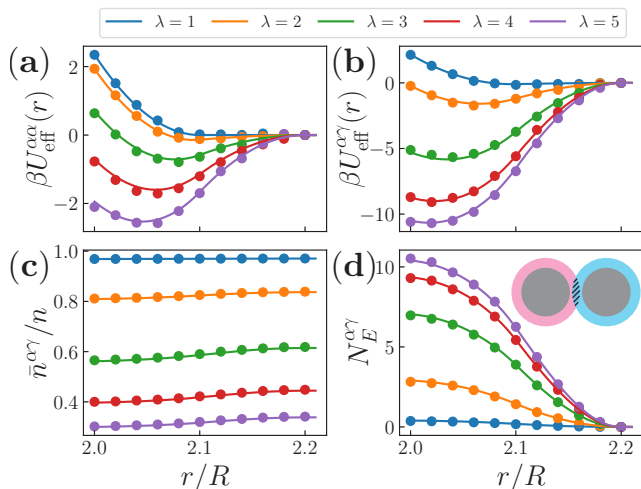


FIG. 2: **Numerical verification of the effective pair interactions between PAEs.** (a,b) EE-mediated effective PAE-PAE interactions  $\beta U_{\text{eff}}(r)$  as functions of the center-to-center distance  $r$  between two PAEs for different EE valency  $\lambda$ , where the PAEs are of the same type (a,  $\beta U_{\text{eff}}^{\alpha\alpha}$ ) and different types (b,  $\beta U_{\text{eff}}^{\alpha\gamma}$ ). (c) The ratio of unbound ssDNAs  $\bar{n}^{\alpha\gamma}/n$  as a function of  $r$  for different  $\lambda$  between PAEs of different types. (d) Number of EEs  $N_E^{\alpha\gamma}$  depicted by the shadow area in the inset as a function of  $r$  for different  $\lambda$  between PAEs of different types. Symbols are from numerical simulations, and curves are theoretical predictions. Parameters:  $\beta\mu = -14$ ,  $\beta\Delta G = -10$ ,  $n = 100$  and  $l_r = 0.1R$ .

deleted using standard GCMC moves [32]. The effective interactions are calculated for a given chemical potential of EEs  $\mu$  and a specified center-to-center distance  $r$  between two PAEs using the thermodynamic integration (see SM Sec. III [31]). As shown in Fig. 2 (a,b), we plot the pair interactions between the same and different types of PAEs,  $\beta U_{\text{eff}}^{\alpha\alpha}$  and  $\beta U_{\text{eff}}^{\alpha\gamma}$ , demonstrating that our method quantitatively agrees with the explicit EE simulations without requiring any fitting parameter. Our method captures the number of unbound ssDNAs on PAEs, i.e.,  $\bar{n}^{\alpha\gamma}/n$  with  $n_\alpha = n_\gamma = n = 100$ , and the number of EEs between two PAEs, i.e.,  $N_E^{\alpha\gamma}$ , and these results also agree quantitatively with the simulation data (Fig. 2(c,d)). Furthermore, our method provides detailed information on EEs in different substates.

*Entropy driven effective PAE-PAE interactions.* Similar to the bivalent linker-mediated DNACCs and polymer-microemulsion networks [16, 33], as shown in Fig. 3(a,b), we observe that the strength of effective colloidal interactions  $\beta U_{\text{eff}}^{\alpha\alpha/\alpha\gamma}(r^* = 2R)$  reaches a plateau at the strong binding energy or low temperature limit ( $\beta\Delta G \rightarrow -\infty$ ). The reason is that at this limit,  $\bar{n}_i \rightarrow 0$ , and all ssDNAs on any PAE  $i$  are occupied. Therefore, for any PAE configurations, the energy part remains the same as the configuration where all PAEs are isolated, and has no contribution to the effective interaction  $\beta U_{\text{eff}}$ .

At this limit,  $\beta U_{\text{eff}}$  solely depends on the combinatorial and configurational entropies, i.e., the valency and chemical potential of EEs. Based on the additional constraint  $\bar{n}_i \rightarrow 0$  and taking the reference state as  $\mathcal{A}^1$ , we introduce the entropy driven effective binding strength of an EEs under  $\mathcal{A}_i^k$  substate,  $\Xi_{\mathcal{A},i}^k$ , and under  $\mathcal{B}_{ij}^{kl}$  substate,  $\Xi_{\mathcal{B},ij}^{kl}$ , respectively (see SM Sec. II [31])

$$\Xi_{\mathcal{A},i}^k = \Xi_{\mathcal{A},i}^k / (\Xi_{\mathcal{A},i}^1)^k = \frac{\binom{\lambda}{k} m_i^0}{(m_i^0 \lambda)^k}, \quad (6a)$$

$$\Xi_{\mathcal{B},ij}^{kl} = \Xi_{\mathcal{B},ij}^{kl} / [(\Xi_{\mathcal{A},i}^1)^k (\Xi_{\mathcal{A},j}^1)^l] = \frac{w^{kl} m_{ij}^0}{(m_i^0 \lambda)^k (m_j^0 \lambda)^l}, \quad (6b)$$

with the free energy of bound EEs

$$\beta F_{\text{att}} = \sum_i \left[ n_i \log \left( \frac{m_i^1}{m_i^0} \right) - M_i - \sum_{j < i} Q_{ij} \right] + \text{const.} \quad (7)$$

To demonstrate the entropy driven PAE-PAE interactions in many-body systems, we perform  $NVT$  MC simulations with the effective interaction from Eq. 1 and 5 for an equimolar binary mixture of PAEs at the packing fraction  $\eta = 4N\pi R^3/3V = 0.094$  with various  $\beta\Delta G$  and  $\lambda$ , where we consider a PAE as a singlet if there is no bridge formed with other PAEs (see SM Sec. III [31]). As shown in Fig. 3 (c), the singlet fraction decreases and reaches a plateau with decreasing  $\beta\Delta G$ , following the same trend as the pair interaction (Fig 3(a,b)).

*Anomalous EE valency dependence.* As shown in Fig. 3(a,b), approaching the strong binding limit ( $\beta\Delta G \rightarrow -\infty$ ), intriguingly, the effective interaction strength between the same type of PAEs,  $\beta U_{\text{eff}}^{\alpha\alpha}(r^*)$ , becomes stronger as the valency of EE  $\lambda$  increases, while the effective interaction between different types of PAEs,  $\beta U_{\text{eff}}^{\alpha\gamma}(r^*)$ , shows the opposite dependence. To clarify these trends, we plot  $\beta U_{\text{eff}}^{\alpha\alpha/\alpha\gamma}(r^*)$  as functions of  $\lambda$  at the strong binding limit, shown as the black solid and dashed curves in Fig. 4. We note that at this limit,  $\bar{n}$  is almost independent of distance, i.e., the number of bridging EEs  $Q$  is small enough, and the effective pair interaction  $\beta U_{\text{eff}}$  mainly depends on  $Q$ , with  $\beta U_{\text{eff}} \approx -Q$ . For the  $\alpha\alpha$  interaction, we have the relation  $Q_{ij}/m_{ij}^0 = M_i M_j / m_i^0 m_j^0$ , i.e.,  $Q_{ij} \sim M_i M_j$ , indicating that bridging is a joint event depending on the adsorption on both particles, where adsorption promotes bridging. Therefore, as  $\lambda$  increases, both the numbers of EEs in the adsorbed state and bridging state decrease, leading to a weaker effective EE-mediated interaction. Differently, for the  $\alpha\alpha$  interaction, we have  $Q_{ij} \sim -M_i - M_j$ , indicating that bridging competes with adsorption. Thus, increasing the  $\lambda$  decreases the number of EEs in the adsorbed state while increasing the number of EEs in the bridging state, resulting in a stronger effective PAE interaction.

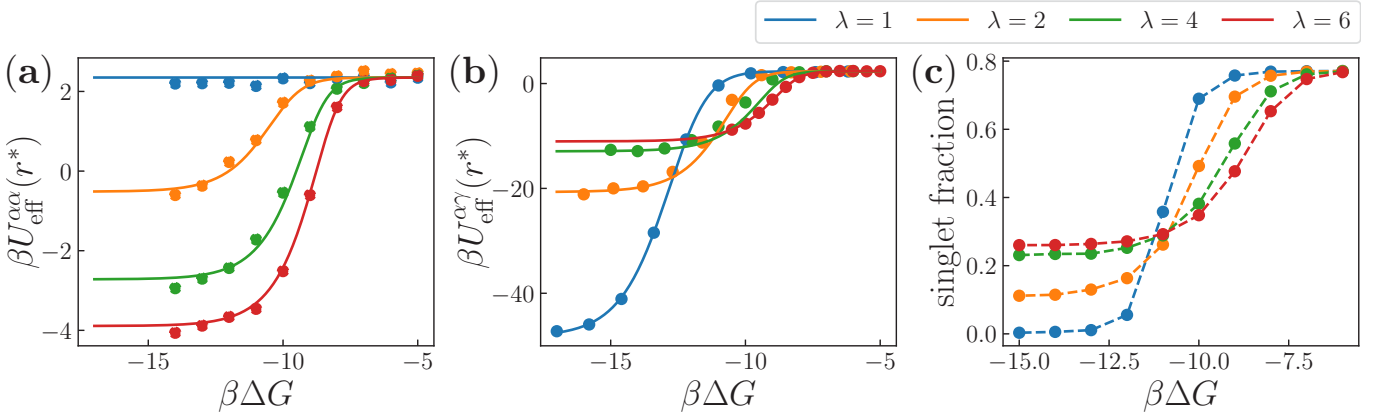


FIG. 3: **Entropy driven PAE-PAE interactions** (a,b) The strength of EE-mediated interaction  $\beta U_{\text{eff}}(r^*)$  as functions of individual binding energy  $\beta\Delta G$  between two PAEs for different EE valency  $\lambda$  at  $\beta\mu = -13$ , where the PAEs are of the same type (a,  $\beta U_{\text{eff}}^{\alpha\alpha}(r^*)$ ) and different types (b,  $\beta U_{\text{eff}}^{\alpha\gamma}(r^*)$ ). Symbols are from numerical simulations, and curves are theoretical predictions. (c) Singlet fraction in manybody PAE-EEs systems at  $\eta = 0.094$  as a function of  $\beta\Delta G$  for different  $\lambda$  at  $\beta\mu = -11$ . Parameters:  $n_\alpha = n_\gamma = 100$ ,  $r^* = 2R$  and  $l_r = 0.1R$ .

Furthermore, we observe that with increasing  $\lambda$ , indicated by the gray horizontal line in Fig. 4, the effective PAE interactions unexpectedly converge and become independent of the binding energy and the type of pairs. At this limit, we also have  $\bar{n}_i \rightarrow 0$ , similar to the strong binding limit according to Eq. 4. Thus,  $\beta F_{\text{att}}$  in Eq. 7 holds with the effective binding strength (see SM Sec. II [31])

$$\tilde{m}_{\mathcal{A},i}^k = \frac{m_i^0}{k!(m_i^0)^k}, \quad \tilde{m}_{\mathcal{B},ij}^{kl} = \frac{m_{ij}^0}{k!l!(m_i^0)^k(m_j^0)^l}. \quad (8)$$

This indicates that increasing the valency has less and less impact on effective PAE interactions.

At finite binding energies, the effect of increasing  $\lambda$  depends on the types of PAEs involved. As shown in Fig. 4, for interactions between the same type of PAEs ( $\beta U_{\text{eff}}^{\alpha\alpha}$ ), increasing the EE valency leads to stronger interactions that eventually converge, similar to the behavior in the strong binding limit. Differently, the situation is more complex for interactions between different types of PAEs ( $\beta U_{\text{eff}}^{\alpha\gamma}$ ). At weak binding energies, e.g.,  $\beta\Delta G = -10$ , increasing  $\lambda$  strengthens the PAE-PAE interaction; at strong binding energies, e.g.,  $\beta\Delta G = -14$ , increasing the EE valency weakens the PAE-PAE interaction; and at intermediate binding energies, e.g.,  $\beta\Delta G = -12$ , the dependence of the strength of PAE-PAE interaction on  $\lambda$  is non-monotonic. Stronger binding energies cause the effective interaction to more closely resemble that of the strong binding limit, whereas weaker binding energies result in PAE-PAE interactions that are naturally weaker than this limit.

As all interactions converge at large  $\lambda$ , one can find that there exists an optimal valency  $\lambda^*$  at which the difference between strengths of effective interactions among different PAEs  $|\beta U_{\text{eff}}^{\alpha\gamma}(r^*) - \beta U_{\text{eff}}^{\alpha\alpha}(r^*)|$  maximizes, and  $\lambda^*$  decreases with decreasing the binding free energy  $\Delta G$

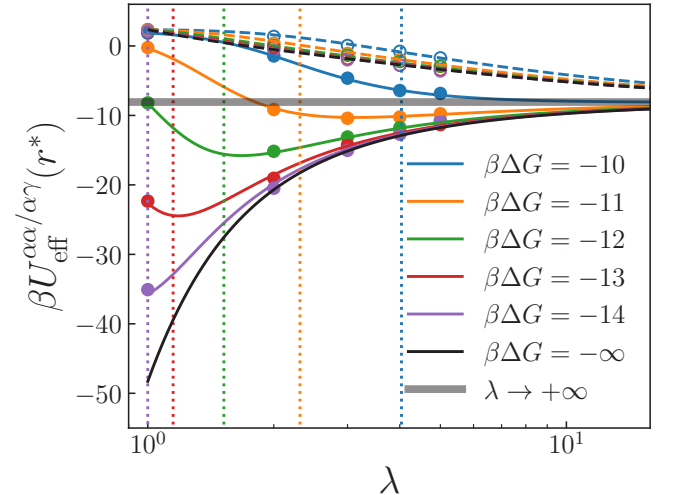


FIG. 4: **Anomalous  $\lambda$  dependence of effective interaction.** The strength of EE-mediated interactions between PAEs of the same type ( $\beta U_{\text{eff}}^{\alpha\alpha}$ , dashed curves and open symbols) and the different types same type ( $\beta U_{\text{eff}}^{\alpha\gamma}$ , solid curves and solid symbols) as functions of EE valency  $\lambda$  with different binding energy  $\beta\Delta G$ . Symbols are calculated from numerical simulations. The vertical dotted lines show the location of optimal valency  $\lambda^*$  where  $|\beta U_{\text{eff}}^{\alpha\gamma}(r^*) - \beta U_{\text{eff}}^{\alpha\alpha}(r^*)|$  maximizes at different  $\beta\Delta G$ . The horizontal grey line indicates  $\beta U_{\text{eff}}(r^*)$  at large  $\lambda$  limit. Parameters:  $\beta\mu = -13$ ,  $n = 100$ ,  $r^* = 2R$  and  $l_r = 0.1R$ .

(Fig. 4). This optimal  $\lambda$  maximizes the disparity between targeted ( $\alpha\gamma$ ) and non-targeted ( $\alpha\alpha$ ) PAE interactions, and our results suggest that at the strong binding limit ( $\Delta G \rightarrow -\infty$ ), the optimal valency of EE for mediating specific binding between targeted PAEs is  $\lambda^* = 1$ . However, we note that experimentally the binding strength is normally not very strong, as strong binding would make

the system hard to reach the designed state in equilibrium.

*Discussion.* To conclude, we have studied the self-assembly of a minimal binary system of PAE-EEs, where EEs act as multivalent linkers with two types of ssDNA ends complementary to those on PAEs. We derived an explicit formula for the effective PAE-PAE interaction mediated by EEs with arbitrary valency  $\lambda$ , which quantitatively agrees with simulations incorporating explicit EEs. Our analysis reveals an anomalous dependence of the effective PAE-PAE interactions on  $\lambda$ . Specifically, at the strong binding limit, we found that increasing  $\lambda$  strengthens the interaction between PAEs of the same type but weakens that between different types, which converges to the same value in the large valency limit. We identified an optimal valency  $\lambda^*$  that maximizes the effective interaction difference between the targeted and non-targeted PAE pairs, which provides a practical design principle for the designed self-assembly of PAE-EE systems. Moreover, our explicit formula can be directly used in MC simulation to efficiently sample the thermodynamic and structural information of the system. Beyond motivating experimental work towards the design of complex DNA structures, we provide the tools for modeling and analyzing soft matter and biological systems with multivalent linkers, e.g., polyelectrolyte [34, 35], hydrogels [36, 37], vitrimers [38, 39], multivalent drug design [40, 41], and cell adhesion and signaling [42].

X. X. acknowledges support from the Alexander von Humboldt-Stiftung. This work was financially supported by the Academic Research Fund from the Singapore Ministry of Education (RG151/23 and MOE2019-T2-2-010) and the National Research Foundation, Singapore, under its 29th Competitive Research Program (CRP) Call (NRF-CRP29-2022-0002).

---

\* These authors contributed equally.

† Electronic address: r.ni@ntu.edu.sg

- [1] M. R. Jones, N. C. Seeman, and C. A. Mirkin, *Science* **347**, 1260901 (2015).
- [2] C. Mirkin, R. Letsinger, R. Mucic, and J. Storhoff, *Nature* **382**, 607 (1996).
- [3] A. Alivisatos, K. Johnsson, X. Peng, T. Wilson, C. Loweth, M. Bruchez Jr, and P. Schultz, *Nature* **382**, 609 (1996).
- [4] C. R. Laramy, M. N. O'Brien, and C. A. Mirkin, in *Spherical Nucleic Acids* (Jenny Stanford Publishing, 2020), pp. 227–289.
- [5] S. Mura, J. Nicolas, and P. Couvreur, *Nat. Mater.* **12**, 991 (2013).
- [6] Q. Hu, H. Li, L. Wang, H. Gu, and C. Fan, *Chem. Rev.* **119**, 6459 (2018).
- [7] T. A. Taton, C. A. Mirkin, and R. L. Letsinger, *Science* **289**, 1757 (2000).
- [8] Y. C. Cao, R. Jin, and C. A. Mirkin, *Science* **297**, 1536 (2002).
- [9] X. Xia and R. Ni, *Phys. Rev. Lett.* **132**, 118202 (2024).
- [10] A. F. Radovic-Moreno, N. Chernyak, C. C. Mader, S. Nallagatla, R. S. Kang, L. Hao, D. A. Walker, T. L. Halo, T. J. Merkel, C. H. Rische, et al., *Proc. Natl. Acad. Sci. U.S.A.* **112**, 3892 (2015).
- [11] S. Wang, L. Qin, G. Yamankurt, K. Skaku, Z. Huang, P.-C. Chen, D. Dominguez, A. Lee, B. Zhang, and C. A. Mirkin, *Proc. Natl. Acad. Sci. U.S.A.* **116**, 10473 (2019).
- [12] P. L. Biancaniello, A. J. Kim, and J. C. Crocker, *Phys. Rev. Lett.* **94**, 058302 (2005).
- [13] H. Xiong, D. Van Der Lelie, and O. Gang, *Phys. Rev. Lett.* **102**, 015504 (2009).
- [14] Y. Zhang, S. Pal, B. Srinivasan, T. Vo, S. Kumar, and O. Gang, *Nat. Mater.* **14**, 840 (2015).
- [15] J. Lowensohn, B. Oyarzún, G. Narváez Paliza, B. M. Mognetti, and W. B. Rogers, *Phys. Rev. X* **9**, 041054 (2019).
- [16] X. Xia, H. Hu, M. P. Ciamarra, and R. Ni, *Sci. Adv.* **6**, eaaz6921 (2020).
- [17] T. Kwon, T. A. Wilcoxson, D. J. Milliron, and T. M. Truskett, *J. Chem. Phys.* **157** (2022).
- [18] M. Girard, S. Wang, J. S. Du, A. Das, Z. Huang, V. P. Dravid, B. Lee, C. A. Mirkin, and M. Olvera de la Cruz, *Science* **364**, 1174 (2019).
- [19] Y. Lin and M. Olvera De La Cruz, *Phys. Rev. E* **101**, 032603 (2020).
- [20] A. Ehlen, H. Lopez-Rios, and M. Olvera de la Cruz, *Phys. Rev. Materials* **5**, 115601 (2021).
- [21] H. Lopez-Rios, A. Ehlen, and M. Olvera de la Cruz, *The J. Phys. Chem. C* **125**, 1096 (2021).
- [22] Y. Lin and M. Olvera de la Cruz, *The J. Phys. Chem. B* **126**, 6740 (2022).
- [23] H. F. Cheng, S. Wang, and C. A. Mirkin, *J. Am. Chem. Soc.* **143**, 1752 (2021).
- [24] S. Wang, S. Lee, J. S. Du, B. E. Partridge, H. F. Cheng, W. Zhou, V. P. Dravid, B. Lee, S. C. Glotzer, and C. A. Mirkin, *Nat. Mater.* **21**, 580 (2022).
- [25] S. Wang, J. S. Du, N. J. Diercks, W. Zhou, E. W. Roth, V. P. Dravid, and C. A. Mirkin, *J. Am. Chem. Soc.* **141**, 20443 (2019).
- [26] Y. Lin and M. Olvera de la Cruz, *Proc. Natl. Acad. Sci. U.S.A.* **120**, e2300257120 (2023).
- [27] S. Angioletti-Uberti, P. Varilly, B. M. Mognetti, A. V. Tkachenko, and D. Frenkel, *J. Chem. Phys.* **138**, 021102 (2013).
- [28] S. Angioletti-Uberti, P. Varilly, B. M. Mognetti, and D. Frenkel, *Phys. Rev. Lett.* **113**, 128303 (2014).
- [29] L. Di Michele, S. J. Bachmann, L. Parolini, and B. M. Mognetti, *The J. Chem. Phys.* **144** (2016).
- [30] P. Varilly, S. Angioletti-Uberti, B. M. Mognetti, and D. Frenkel, *J. Chem. Phys.* **137**, 094108 (2012).
- [31] Supplementary Material.
- [32] D. Frenkel and B. Smit, *Understanding Mol. Simul.: from algorithms to applications* (Elsevier, 2023).
- [33] A. Zilman, J. Kieffer, F. Molino, G. Porte, and S. Safran, *Phys. Rev. Lett.* **91**, 015901 (2003).
- [34] M. Muthukumar, *Macromolecules* **50**, 9528 (2017).
- [35] J. Yu, N. Jackson, X. Xu, Y. Morgenstern, Y. Kaufman, M. Ruths, J. De Pablo, and M. Tirrell, *Science* **360**, 1434 (2018).
- [36] H. W. Ooi, J. M. Kocken, F. L. Morgan, A. Malheiro, B. Zoetebier, M. Karperien, P. A. Wieringa, P. J. Dijkstra, L. Moroni, and M. B. Baker, *Biomacromolecules*

- 21**, 2208 (2020).
- [37] H. Le Roy, J. Song, D. Lundberg, A. V. Zhukhovitskiy, J. A. Johnson, G. H. McKinley, N. Holten-Andersen, and M. Lenz, *Sci. Adv.* **10**, ead15056 (2024).
- [38] M. Röttger, T. Domenech, R. van Der Weegen, A. Breuillac, R. Nicolaÿ, and L. Leibler, *Science* **356**, 62 (2017).
- [39] Q.-L. Lei, X. Xia, J. Yang, M. Pica Ciamarra, and R. Ni, *Proc. Natl. Acad. Sci. U.S.A.* **117**, 27111 (2020).
- [40] M. Mammen, S.-K. Choi, and G. M. Whitesides, *Angew. Chem. Int. Ed.* **37**, 2754 (1998).
- [41] G. V. Dubacheva, T. Curk, and R. P. Richter, *Acc. Chem. Res.* **56**, 729 (2023).
- [42] J. Zhu, B.-H. Luo, T. Xiao, C. Zhang, N. Nishida, and T. A. Springer, *Mol. Cell* **32**, 849 (2008).